A Mössbauer effect study of combinatorially prepared Al_2O_3/Fe and LiF/Fe multilayers

2008 J. Phys.: Condens. Matter 20 055203

(http://iopscience.iop.org/0953-8984/20/5/055203)

J. Phys.: Condens. Matter **20** (2008) 055203 (9pp) doi:10.1088/0953-8984/20/05/055203

A Mössbauer effect study of combinatorially prepared Al_2O_3/Fe and LiF/Fe multilayers

Peng Liao[1], **R A Dunlap**[1,2] **and J R Dahn**[1,2,3]

[1] Department of Physics and Atmospheric Science, Dalhousie University, Halifax, NS, B3H 3J5, Canada
[2] Institute for Research in Materials, Dalhousie University, Halifax, NS, Canada

E-mail: jeff.dahn@dal.ca

Received 24 October 2007, in final form 9 December 2007
Published 14 January 2008
Online at stacks.iop.org/JPhysCM/20/055203

Abstract

Nanocomposites of lithium fluoride and transition metals have been proposed for use as positive electrode materials in lithium ion batteries. The interface between the two phases is thought to play a very important role in the electrochemical activities of these nanocomposites. In this paper, two Fe/insulator multilayer systems were prepared and investigated by means of small angle x-ray scattering (SAXs), x-ray diffraction and ^{57}Fe Mössbauer spectroscopy measurements. These samples consist of wedges of Fe (between 0 and 1.5 nm thickness) separated by a 2.1 nm constant thickness Al_2O_3 spacer and wedges of Fe (between 0 and 2.0 nm thickness) separated by a 1.6 nm constant thickness LiF spacer. For both Al_2O_3/Fe and LiF/Fe multilayers, SAXs shows Bragg peaks due to modulated superstructures. For the Al_2O_3/Fe multilayers, ^{57}Fe Mössbauer spectra show that three types of Fe exist within the interface region between Fe and amorphous Al_2O_3 layers: γ-Fe with a face centered cubic structure, Fe in interstitial sites within amorphous alumina and an Fe^{2+} species, much like $FeAl_2O_4$. For the LiF/Fe multilayers, ^{57}Fe Mössbauer spectra show that an interfacial region about 0.2–0.3 nm wide exists between the LiF and Fe layers. The data suggest that the Li:F ratio is less than 1 within the interface region, as expected due to 'sharing' of the electronegative F atoms by the two cations. The excess Li ions and electrons are thought to be stored on either side of the interface by a mechanism proposed by Maier and co-workers.

(Some figures in this article are in colour only in the electronic version)

1. Introduction

Nanostructured materials show many novel properties which are not possessed by bulk materials. For example, when nanosized lithium fluoride and transition metals are intimately mixed, these nanocomposites exhibit electrochemical activity as displacement-type positive electrode materials for Li-ion batteries, unlike their bulk counterparts [1, 2]. Recently, Maier and co-workers have shown that the interface between nanograins of Li_2O and transition metals plays an important role in the storage of extra lithium atoms above that expected for the simple displacement reaction [3–6]. Our work [7] also suggests that excess capacity, beyond that expected for the displacement reaction alone, is found in LiF/Fe nanocomposites and that these excess Li atoms could be stored in the interfacial regions. Therefore, it is extremely important to study and understand the interface between LiF and Fe grains in such nanocomposites. Such a study is the focus of the present paper.

When a nanoscale mixture of LiF and a transition metal, M, is used as the positive electrode in lithium ion batteries, the following displacement reaction occurs:

$$n\mathrm{LiF} + \mathrm{M} \leftrightarrow \mathrm{MF}_n + n\mathrm{Li}.$$

During the charge process, the metal is oxidized and metal fluorides are formed, while lithium ions and electrons are

[3] Author to whom any correspondence should be addressed.

extracted from the positive electrode. During the discharge, lithium ions are inserted into the positive electrode and the reaction is reversed so the active material is reduced to the mixture of nanosized lithium fluoride and metal. Because all the oxidation states of the cation of the active material can be used in the reaction, displacement reactions can have specific capacities up to 700 mAh g^{-1}, while the upper limit of the specific capacity of the currently used lithium transition metal oxides is about 280 mAh g^{-1} [8].

Some properties of nanocomposites of lithium fluoride and transition metal are still not clear. The differential capacity versus potential of these materials shows a sharp discharge peak followed by a wide hump (appearing as a sloping region in potential plotted versus capacity). The hump is difficult to explain based on the displacement reaction alone, which should occur at a single potential. Furthermore, the discharge capacities of these nanocomposites are always larger than the theoretical values if we assume that the displacement reaction is the only mechanism for discharge [7, 9, 10]. Similar results were also found when discharging Li/transition metal oxide cells based on displacement reactions [11]. Maier and co-workers suggest that the extra capacity and the associated wide hump in the differential capacity versus potential of Li/RuO_2 cells comes from lithium storage at the interfaces between newly formed Li_2O and Ru grains. Their *ab initio* calculations show that at least one monolayer of additional Li can be stored at each interface between Li_2O and Ru resulting in an extra capacity approaching 100 mA h g^{-1} in their experiments [6].

Ochi *et al* [12] and Kita *et al* [13] prepared Fe/LiF multilayered thin films by ultrahigh-vacuum evaporation methods. Using Mössbauer effect spectroscopy they found that Fe and LiF mixed at the interfaces to form 'imperfect compounds' [12, 13]. However, their work did not focus on the details of the interface, but instead on the magnetic properties of the multilayers.

In this paper, we try to provide experimental proof for the interfacial charge storage mechanism using Mössbauer effect spectroscopy. Mössbauer effect spectroscopy is very sensitive to the environment of Mössbauer active elements such as Fe and Sn. Fe atoms within a large grain and Fe within interfacial regions contribute different components to the total Mössbauer spectrum. By analyzing the site parameters and populations of Fe atoms within the different regions, it is possible to construct a reasonable model of the interface region [14, 15].

We first wanted to study an Fe/insulator system for which results exist in the literature as a trial system. We selected Al_2O_3/Fe since it has been studied before [16, 17]. In addition, we decided to use our combinatorial and high throughput materials science infrastructure to prepare multilayer systems with varying Fe layer thickness [18]. With these methods in place a similar study was then performed on the system of interest, multilayers of nanometer thick LiF and Fe, where the Fe thickness varies from 0 to 1.6 nm. The structure and composition of the libraries were characterized by small angle x-ray scattering (SAXs), wide angle x-ray diffraction (XRD), ^{57}Fe Mössbauer effect spectroscopy and electron microprobe analysis (EMPA). From these studies a detailed picture of the interface region was obtained.

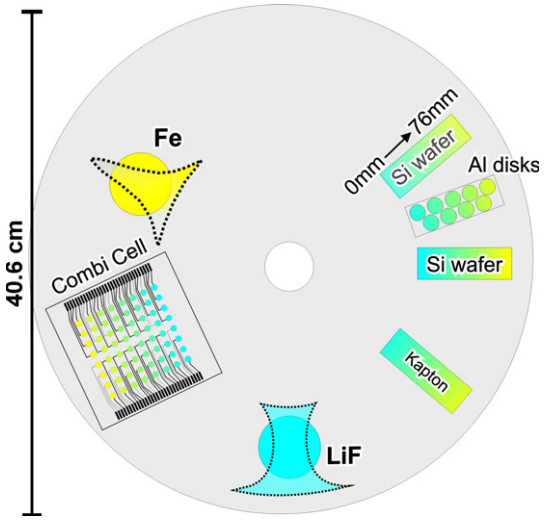

Figure 1. Layout of the combinatorial sputtering table. Substrates mounted include an array of Al foil discs for mass per unit area determination, two silicon substrates and 13 pieces of 25 μm thick kapton film (each 25 mm × 100 mm). Two sputtering targets are also indicated. The Fe target has a 'linear in' mask, while the LiF (or Al_2O_3) target has a 'constant' mask.

2. Experiment

Multilayers of Al_2O_3/Fe and LiF/Fe were made by magnetron co-sputtering using a Corona Vacuum Coater's (Vancouver, BC, Canada) V3T system. A base pressure around 1×10^{-7} Torr was reached before sputtering began. The sputtering chamber is equipped with a 40 cm diameter water-cooled rotating substrate table. Five 50 mm diameter magnetrons are mounted at 60° increments along a circle of radius 13.3 cm which is concentric with the substrate table. Stationary masks are placed over individual targets to control the deposition profiles of the sputtered elements [19]. Deposition was carried out under a flow rate of 5 sccm Argon, yielding a chamber pressure of 1.0 mTorr. The substrate table angular speed was approximately 2.8 rpm.

As shown in figure 1, the LiF and Fe sputtering targets (Al_2O_3 and Fe targets for Al_2O_3/Fe multilayers) were covered with masks designed to give a multilayer thin-film library with the thickness of Fe decreasing approximately linearly outward and the thickness of LiF remaining constant. As the substrate passes over the LiF (or Al_2O_3) and Fe targets very slowly, an average thickness, a, of LiF (or Al_2O_3) molecules is deposited followed by an average thickness, b, of Fe atoms. This process is repeated N times to get a film with N bilayers. We designate this structure by writing LiF/Fe or Al_2O_3/Fe. The thicknesses a and b are referred to as the sublayer thicknesses and the layer thickness, $a + b = d$, is called the superlattice parameter. We shall also use Λ to designate the composition modulation wavelength. Details of the sputtering procedure and modifications to the machine to enable combinatorial sputtering have been previously described [19]. For all films discussed in this paper, Al_2O_3 was deposited using a radio frequency (RF) power supply with a power of 200 W, LiF was deposited using a radio frequency (RF) power supply with a

power of 160 W. The Fe target was powered by a DC power supply at 30 W.

Al_2O_3/Fe and LiF/Fe multilayers were deposited on two Si(100) wafers, a linear array of 13 mm diameter pre-weighed Al foil discs, and 13 pieces of 25 μm thick kapton film (each 25 mm × 100 mm) for the Mössbauer measurements [19]. One Si wafer was used to determine the bilayer thickness using SAXs and the other Si wafer was used for x-ray diffraction studies of the deposited material. The Al foil discs were used to determine the mass per unit area deposited as a function of position on the library. Weights were measured before and after sputtering using a Cahn 29 microbalance.

A Siemens D-5000 diffractometer, equipped with a Cu target x-ray tube and a diffracted beam monochromator was used for the SAXs studies of selected points on the film. In order to limit the extent of beam on the sample, the 76 mm long library was cleaved into separate 5 mm width pieces and 0.1° divergence slits were used. This was done since the superlattice parameter varies with position along the library, so if the beam spans a long section of the library, the superlattice peaks become exceedingly broad. The D-5000 uses θ–θ Bragg–Brentano geometry so that the scattering vector is always perpendicular to the film.

Films deposited on the other Si wafer substrate were used in wide angle XRD experiments to determine the structure as a function of position across the film. XRD measurements were performed using an INEL CPS120 curved position sensitive detector coupled to an x-ray generator equipped with a Cu target x-ray tube. A monochromator in the incident beam path limits the wavelengths striking the sample to Cu Kα. The detector measures the entire diffraction pattern between scattering angles of 6° and 120° at once. The film sample is placed on an x–y translation stage that allows measurement and movement operations to be sequentially programmed. Typically, XRD data were collected over the 76 mm long libraries with a spacing of 4 mm, leading to 19 patterns per library. Typical measurement times were 20 min per point on the library. The x-ray beam makes a spot about 1 mm (in the varying composition direction) by 3 mm (in the constant composition direction) in size on the library.

Room temperature ^{57}Fe Mössbauer effect spectra were collected using a Wissel System II spectrometer operating in the constant acceleration mode. A Rh^{57}Co source was used and the velocity scale was calibrated relative to room temperature α-Fe. Thirteen layers of film deposited onto Kapton substrates were compositionally aligned and attached together to form the absorber. The absorber was then moved inside a helium-filled glove box and sealed between aluminized polyester sheets with a heat sealer to prevent subsequent air exposure during the extended time needed to collect all the Mössbauer spectra. Spectra were obtained by moving the sample in front of a 4.5 mm × 25 mm lead aperture. Approximately a 6% range of the full composition spread was sampled at each step by using the 4.5 mm aperture. Data acquisition times at each position were typically 24–36 h. More details of the combinatorial Mössbauer technique are available in the literature [20].

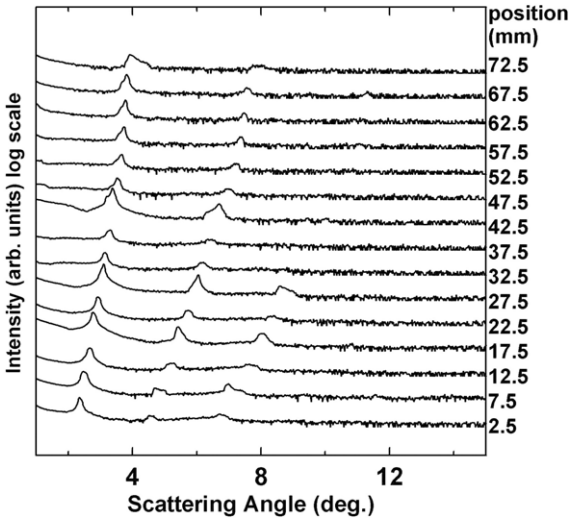

Figure 2. Small angle x-ray scattering patterns (SAXs) collected from nineteen different positions along the Al_2O_3/Fe multilayer libraries. The left y-axis is the x-ray intensity on a log scale and the right y-axis indicates the position in the 76 mm long library.

3. Results and discussion

3.1. Al_2O_3/Fe multilayers

Small angle x-ray scattering (SAXs) was measured to obtain the composition modulation wavelength, Λ, of the Al_2O_3/Fe multilayers. The position of the peaks is given by [21]:

$$\sin^2\theta = \left[\frac{n\lambda_x}{2\Lambda}\right]^2 + 2\overline{\delta_s} \tag{1}$$

where θ is Bragg angle of the peak, n is the order of reflection, λ_x is the x-ray wavelength, Λ is the composition modulation wavelength, and $1 - \delta_s$ is the real part of the average index of refraction of the superlattice. The value of $\overline{\delta_s}$ is typically $\approx 3 \times 10^{-5}$, which only leads to significant deviations for 2θ values less than 3° for Cu radiation. In our calculation we will ignore the influence of $\overline{\delta_s}$, thus equation (1) reduces to:

$$\sin\theta = \frac{n\lambda_x}{2\Lambda}. \tag{2}$$

Figure 2 shows the small angle x-ray scattering patterns of Al_2O_3/Fe multilayers. The positions along the library where the SAXs patterns were collected are labeled to the right of each pattern. Figure 2 shows that the Al_2O_3/Fe multilayers have well-defined Bragg reflections out to third order. Higher order Bragg reflections may be absent because Al_2O_3 and Fe react with each other at the interface, leading to interface roughness. A similar effect has been reported in the literature, where rough interfaces hindered the observation of higher order Bragg reflections from sputtered Nb/Si multilayers [22]. The Bragg peak scattering angles increase across the library, indicating that the Al_2O_3 and Fe bilayer thickness decreases across the library as expected.

It is important to verify that the sputtered library matches the target of the deposition. We assume that the number of

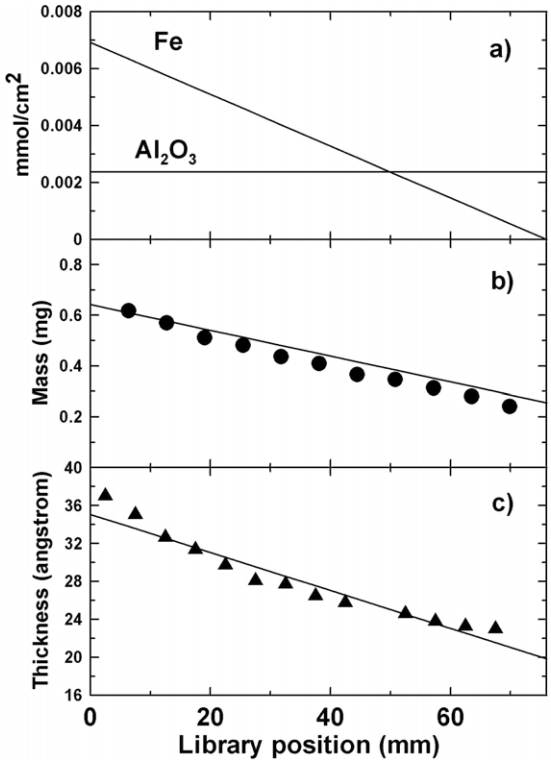

Figure 3. (a) The moles per unit area of Al_2O_3 and Fe defined by the 'constant' and 'linear in' sputtering masks, respectively. (b) The measured mass of the sputtered film on each weighing disc (data points) compared to that calculated from the curves in panel (a) (solid line). (c) Superlattice periodicity, Λ, of the Al_2O_3/Fe multilayers calculated from mass per unit area, density and sputtering table angular velocity (solid curve) compared to Λ measured using small angle x-ray scattering (data points).

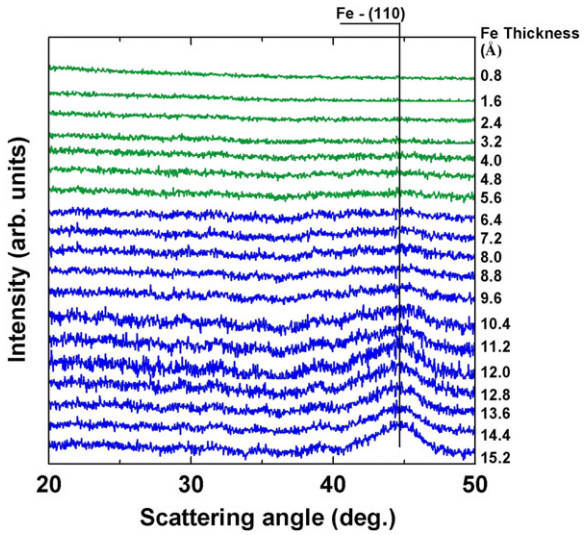

Figure 4. Wide angle XRD patterns collected at different positions along the Al_2O_3/Fe multilayer library on the silicon substrate. The graph shows the x-ray intensity on the left y-axis and an estimate of Fe sublayer thickness for each pattern determined from figure 3(c) on the right y-axis.

moles cm^{-2} of Al_2O_3 is a constant, B, across the 76 mm library, due to the constant mask used, and that the number of moles of Fe decreases linearly from a maximum value, A, at the start of the library to zero at the end of the library due to the 'linear in' mask used. Figure 3(a) shows these variations. The mass per unit area can then be calculated in terms of A and B as a function of library position, y, where 0 mm $< y <$ 76 mm using equation (3):

$$\text{Mass/area} = \left[A * \left(\frac{76 - y}{76}\right) * (55.85) + B * (101.96)\right] \quad (3)$$

where 76 mm is the length of the library, and 55.85 and 101.96 g mol^{-1} are the molar masses of Fe and Al_2O_3. The constants A and B are then used in equation (4) to calculate the period, Λ, of the composition modulation of the Al_2O_3/Fe multilayers:

$$\Lambda = 10^8 * \frac{A * \left(\frac{76-y}{76}\right) * \left(\frac{55.85}{7847}\right) + B * \left(\frac{101.96}{4000}\right)}{\frac{3.14*\left(\frac{1.27}{2}\right)^2*2.8}{(11*60+53)}}. \quad (4)$$

In equation (4), 7847 kg m^{-3} and 4000 kg m^{-3} are the densities of Fe and bulk Al_2O_3. The diameter of the Al weighing discs is 1.27 cm. The total sputtering time was 11 h and 53 min and the angular velocity of the substrate table was 2.8 rpm. The parameters, A and B, were then adjusted to give the best least squares fit to the data for the mass per unit area in figure 3(b) and the composition modulation period, Λ, in figure 3(c). The good agreement between the modeled and measured values in figures 3(b) and (c) shows that the combinatorial sputtering process to produce these multilayers is well understood.

Figure 4 shows 19 XRD patterns collected at different positions along the Al_2O_3/Fe multilayer library on the silicon substrate. The graph shows the x-ray intensity on the left y-axis and an estimate of the thickness of the Fe sublayer on the right y-axis for each pattern determined from the mass per unit area. The total thickness of the Al_2O_3/Fe multilayer film ranges from approximately 900 nm at the thick Fe end to about 500 nm at the pure Al_2O_3 end. For the XRD pattern collected from material containing a 15.2 Å thick Fe sublayer, the broad peak at 44.7° is attributed to the Fe(110) Bragg peak. As Fe thickness decreases, the intensity of the Fe(110) peak decreases. For the material with a 0.8 Å average thickness Fe sublayer, no diffraction peak was observed, which means the sputtered Al_2O_3 sublayers are amorphous.

Figure 5 shows the Mössbauer spectra of various members of the Al_2O_3/Fe multilayer library as a function of Fe sublayer thickness. From 14.8 to 11.2 Å thick Fe sublayers, each Mössbauer spectrum was fit to an asymmetric sextet, a singlet and a doublet with Voigt-based functions (VBF) [23]. The parameters of these components are listed in table 1. The errors of the center shift and internal magnetic field are indicated in parentheses next to the parameters. Some parameters were fixed in order to get a consistent physical model to explain the Mössbauer spectra. Table 1 shows that the singlet has a negative center shift, which is a typical property of fcc γ-Fe, and has been reported before [14]. The center shift and quadrupole splitting of the doublet is very close to Fe^{2+} in

Table 1. Site parameters for Al_2O_3/Fe multilayers.

	$FeAl_x$				Doublet		
Fe thickness (Å)	Center shift (mm s^{-1})[a]	$H(T)$	x	Fraction (%)	Center shift (mm s^{-1})[a]	Quadrupole splitting (mm s^{-1})	Fraction (%)
14.8	0.01 (±0.01)	31.3 (±0.3)	0.02	95.4	0.97 (±0.14)	1.46 (±0.23)	3.4
13.0	0.02 (±0.02)	31.0 (±0.2)	0.03	93.6	0.94 (±0.12)	1.45 (±0.21)	4.3
11.2	0.02 (±0.02)	30.1 (±0.2)	0.06	88.7	0.87 (±0.02)	1.32 (±0.03)	8.1
9.4	0.04 (±0.02)	27.9 (±0.2)	0.10	83.0	0.86 (±0.06)	1.51 (±0.20)	12.3
7.6	0.09 (±0.03)	18.3 (±0.7)	0.11	79.8	0.85 (fixed)	1.49 (±0.25)	13.3
5.8	—	—	—	—	0.85 (fixed)	1.65 (fixed)	15.9
4.0	—	—	—	—	1.07 (±0.08)	1.65 (fixed)	7.7
2.2	—	—	—	—	0.92 (fixed)	1.65 (fixed)	17.6

	Singlet 1		Singlet 2		Singlet 3	
Fe thickness (Å)	Center shift (mm s^{-1})[a]	Fraction (%)	Center shift (mm s^{-1})[a]	Fraction (%)	Center shift (mm s^{-1})[a]	Fraction (%)
14.8	−0.35 (±0.05)	1.3	—	—	—	—
13.0	−0.28 (±0.08)	2.0	—	—	—	—
11.2	−0.29 (±0.02)	3.1	—	—	—	—
9.4	−0.23 (±0.16)	2.1	0.10 (±0.04)	2.6	—	—
7.6	−0.20 (fixed)	1.0	0.06 (fixed)	5.9	—	—
5.8	−0.21 (±0.04)	12.5	0.06 (fixed)	42.1	0.39 (±0.07)	29.4
4.0	−0.20 (±0.01)	16.3	0.06 (fixed)	50.6	0.7 (±0.07)	25.4
2.2	−0.17 (±0.07)	12.9	0.07 (±0.02)	48.8	0.58 (±0.07)	20.7

[a] Center shift was calibrated relative to room temperature α-Fe.

$FeAl_2O_4$ [24]. When fitting the asymmetric sextet, a single Gaussian distribution of Zeeman magnetic splittings was used with a linear correlation between the center shift, δ, and the internal magnetic field, H, of the form:

$$\delta = \delta_0 + \delta_1 H \tag{5}$$

where δ_0 and δ_1 were fitted parameters. Table 1 shows that the center shifts of the asymmetric sextet are positive and their internal magnetic fields are less than 32 T, different from pure BCC Fe (CS = 0 and H = 33 T). As the Fe sublayer thickness decreases, the center shift increases and the internal magnetic field decreases. Similar results have been found in $FeAl_x$ alloys, where x is very small, in mechanically alloyed Fe–Al samples [25]. When there are impurities within bcc Fe, the Fe atoms can have one or more impurities as their eight nearest neighbors. This asymmetric environment will influence the center shift and internal magnetic field of bcc Fe and results in an asymmetric sextet component in the Mössbauer spectrum. From the parameters of the asymmetric sextet it appears that some Al atoms have diffused into the Fe sublayers and that an $FeAl_x$ (x is very small) phase has been formed.

Based on the above analysis, we believe that the following reaction occurs at the interface between the Fe and Al_2O_3 sublayers:

$$(3x + 2 + z)\,(\alpha - \mathrm{Fe}) + 4x\,[Al_2O_3] \rightarrow 3x\,[FeAl_2O_4] + 2FeAl_x + z(\gamma - \mathrm{Fe}). \tag{6}$$

According to equation (6), x in $FeAl_x$ can be estimated by setting the ratio of the doublet population ($FeAl_2O_4$) to the sextet population ($FeAl_x$) equal to $3x/2$. The calculated values of x, which are listed in table 1, are very close to those in [26].

When the Fe sublayer thickness falls below 7.6 Å, each Mössbauer spectrum was fit to three singlets and a doublet. The parameters of these components are also listed in table 1. The singlet with negative center shift is assigned to fcc γ-Fe while the doublet corresponds to $FeAl_2O_4$. The singlet with smaller positive center shift is assigned to superparamagnetic $FeAl_x$ which is located at the center of the Fe sublayer. When the thickness of the central $FeAl_x$ sublayer is very small, the Fe atoms in this phase are superparamagnetic, not ferromagnetic. Superparamagnetic Fe atoms show a singlet in the Mössbauer spectra while ferromagnetic Fe atoms exhibit a sextet. The singlet with larger positive center shift is believed to arise from Fe atoms that diffuse into the amorphous Al_2O_3 sublayer.

Figure 6 shows a schematic model of the nanostructure of the Al_2O_3/Fe multilayers based on the interpretation of the Mössbauer effect spectra. The width of the Fe sublayer between Al_2O_3 spacer sublayer is drawn to scale. Within the interfacial region between the Fe sublayer and the amorphous Al_2O_3 sublayer, small grains of fcc γ-Fe and $FeAl_2O_4$ are mixed with Fe atoms within amorphous Al_2O_3. A small amount of Al atoms diffuse into the central Fe sublayer leading to the $FeAl_x$ phase. This $FeAl_x$ sublayer shows superparamagnetic properties at the thin Fe end of the library.

3.2. LiF/Fe multilayers

Similar to studies on the Al_2O_3/Fe multilayer library, small angle x-ray scattering, wide angle XRD and Mössbauer effect spectroscopy were used to characterize the LiF/Fe multilayer library. Figure 7 shows the SAXs patterns collected at various positions along the LiF/Fe multilayer library. The position where the SAXs data was collected is labeled to the right of

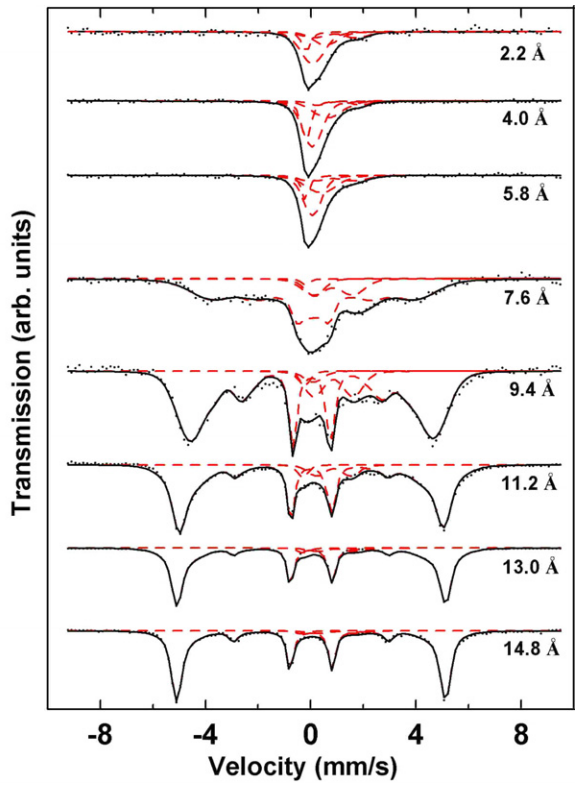

Figure 5. Room temperature ^{57}Fe Mössbauer spectra of the Al_2O_3/Fe multilayer library as a function of Fe content. The velocity scale is measured relative to room temperature α-Fe. The thickness of the Fe sublayer is shown below each spectrum. Solid lines through the data represent the total fits and the dashed lines are the spectral components.

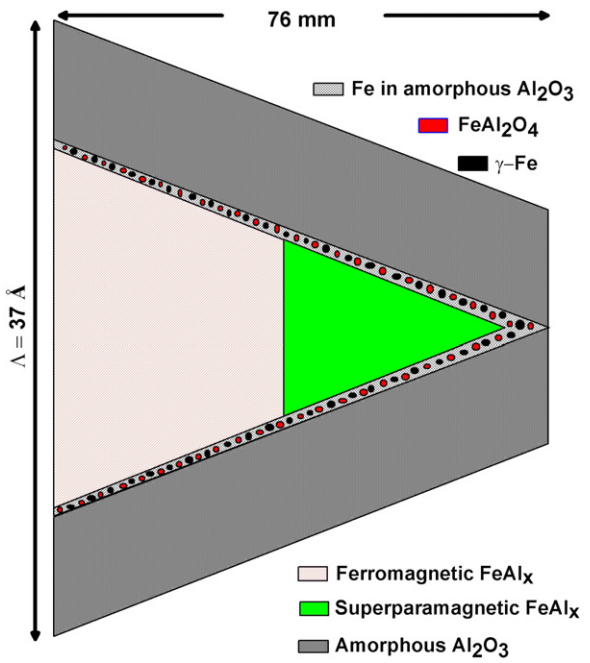

Figure 6. Schematic diagram of the structure of the Al_2O_3/Fe multilayer library. The width of the interfacial region and Fe layer were estimated from the site populations of the relative components in the Mössbauer spectra. The vertical and horizontal scales in the diagram are vastly different.

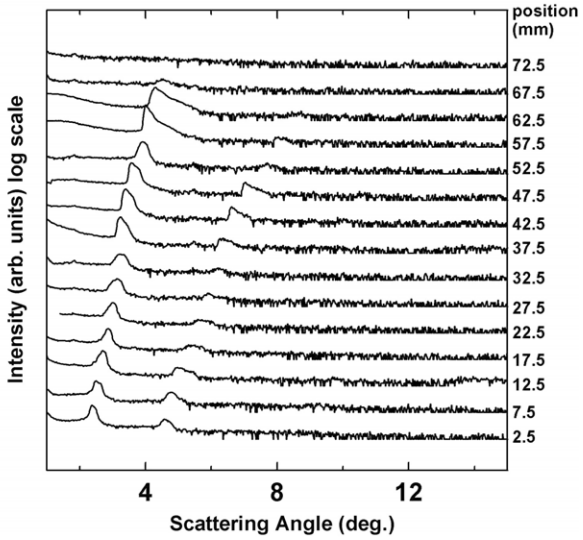

Figure 7. Small angle x-ray scattering patterns (SAXs) collected from nineteen different positions along the LiF/Fe multilayer libraries. The left y-axis is the x-ray intensity on a log scale and the right y-axis indicates the position in the 76 mm long library.

each SAXs pattern. Similar to the Al_2O_3/Fe multilayer library, only two orders of Bragg peaks are observed. Any interfacial reaction between the LiF spacer sublayers and the Fe sublayers will reduce the sharpness of the interface and reduce the higher order SAXs peaks.

Figure 8(a) shows the number of moles cm^{-2} for Fe and for LiF versus library position inferred by fitting to the mass per unit area (figure 8(b)) and the composition modulation wavelength modulation, Λ, (figure 8(c)) using the procedure as was described above for figure 3. Figure 8 shows the behavior expected for a 'constant mask' covering the LiF target and a 'linear in' mask covering the Fe target.

Figure 9 shows 19 wide angle XRD patterns collected at different positions along the LiF/Fe multilayer library on the silicon substrate. An estimate of the Fe sublayer thickness for each pattern determined from the solid line in figure 8(c) is given on the right y-axis of figure 9. The total thickness of the LiF/Fe multilayer thin-film library ranges from approximately 840 nm at the thick Fe end to about 370 nm at the pure LiF end. The XRD pattern collected from material with 21.3 Å thick Fe sublayers, shows a broad peak at 44.7° which is attributed to the Fe(110) Bragg peak. As the Fe sublayer thickness decreases, the intensity of the Fe(110) Bragg peak decreases. For the material with 1.1 Å (average) thick Fe sublayers, the peak at 38.4° is attributed to the LiF(111) Bragg peak. This relatively sharp peak presumably forms because the intervening Fe sublayers are not complete and larger regions of LiF can form. The wide angle XRD patterns are basically amorphous for Fe sublayer thicknesses between 4.5 and 6.7 Å since the sublayers are so thin and because the Fe sublayers are complete enough to prevent the formation of large regions of LiF.

Figure 10 shows Mössbauer spectra collected at various positions along the LiF/Fe multilayer library. The thickness

Table 2. Site parameters for LiF/Fe multilayers

Fe thickness (Å)	Sextet			Doublet			Singlet	
	Center shift (mm s^{-1})[a]	$H(T)$	Fraction (%)	Center shift (mm s^{-1})[a]	Quadrupole splitting (mm s^{-1})	Fraction (%)	Center shift (mm s^{-1})[a]	Fraction (%)
20.7	0.01 (±0.00)	32.4 (±0.1)	97.1	1.23 (±0.11)	2.60 (±0.22)	2.9	—	—
18.2	0.01 (±0.00)	31.6 (±0.1)	95.1	1.24 (±0.08)	2.56 (±0.16)	4.9	—	—
15.6	0.02 (±0.00)	31.1 (±0.1)	84.4	1.03 (±0.17)	1.83 (±0.22)	9.0	0.0 (fixed)	6.6
13.1	0.00 (fixed)	29.0 (±0.2)	78.1	1.26 (fixed)	1.98 (fixed)	8.5	0.0 (fixed)	13.4
10.6	0.00 (fixed)	25.2 (±0.7)	63.8	1.56 (±0.05)	1.31 (±0.08)	13.3	0.0 (fixed)	22.9
8.1	—	—	—	1.44 (±0.01)	1.53 (±0.02)	34.7	0.0 (fixed)	65.3
5.5	—	—	—	1.41 (±0.04)	1.68 (±0.07)	39.8	0.0 (fixed)	60.2
3.0	—	—	—	1.38 (±0.04)	1.80 (±0.07)	65.8	0.0 (fixed)	34.2
0.5	—	—	—	1.31 (±0.01)	1.80 (±0.02)	69.7	0.0 (fixed)	30.3

[a] Center shift was calibrated relative to room temperature α-Fe.

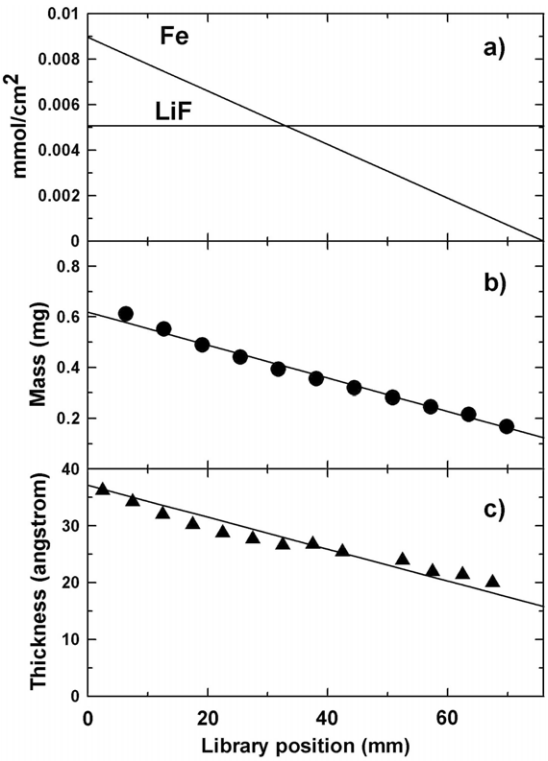

Figure 8. (a) The moles per unit area of LiF and Fe defined by the 'constant' and 'linear in' sputtering masks, respectively. (b) The measured mass of the sputtered film on each weighing disc (data points) compared to that calculated from the curves in panel (a) (solid line). (c) Superlattice periodicity, Λ, of the LiF/Fe multilayers calculated from mass per unit area, density and sputtering table angular velocity (solid curve) compared to Λ measured using small angle x-ray scattering (data points).

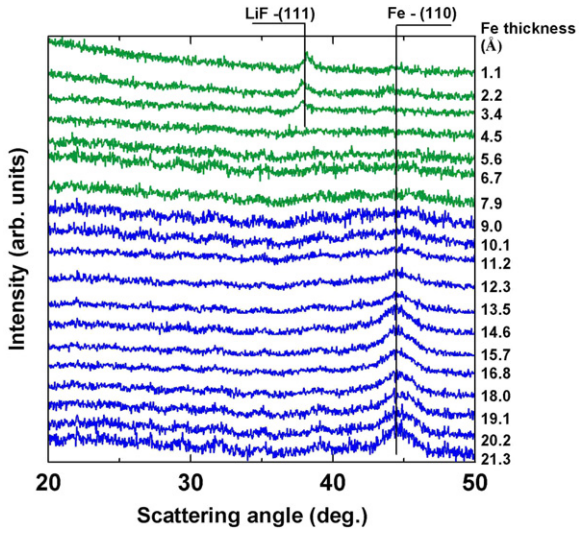

Figure 9. Wide angle XRD patterns collected at different positions along the LiF/Fe multilayer library on the silicon substrate. The graph shows the x-ray intensity on the left y-axis and an estimate of Fe sublayer thickness for each pattern determined from figure 8(c) on the right y-axis.

of the Fe sublayer is indicated next to each spectrum. For Fe sublayers between 18.2 and 20.7 Å each Mössbauer spectrum was fit to a symmetric sextet and a doublet with Voigt-based functions (VBF) [23]. The parameters of these components are listed in table 2. The errors of the center shift and internal magnetic field are indicated in parentheses next to the parameters. Some parameters were fixed in order to get a consistent physical model to explain the Mössbauer spectra. According to the center shift and internal magnetic field of the sextet, the symmetric sextet can be attributed to bcc Fe (CS = 0 and H = 33 T). This suggests that little or no Li or F is incorporated in the centers of the Fe sublayers. Similar to $FeAl_2O_4$ within the interfacial region of the Al_2O_3/Fe multilayer library, the doublet component needed to fit the spectra in figure 10 was assigned to Fe atoms in the interfacial region. The center shift of the doublet from the Fe atoms within interfacial region ranges from 1.03 to 1.44 mm s^{-1}, suggesting that these Fe atoms have been oxidized and have donated some electrons to neighboring F atoms. This indicates that within the interfacial region the Li:F ratio is understoichiometric (<1).

There may be many reasons for the understoichiometric Li:F ratio within the interfacial region. In order to verify that Li atoms are not lost during sputtering LiF, pure LiF was sputtered onto a silicon substrate and characterized visually and by XRD. The sputtered film was transparent immediately after sputtering as expected for stoichiometric LiF and the

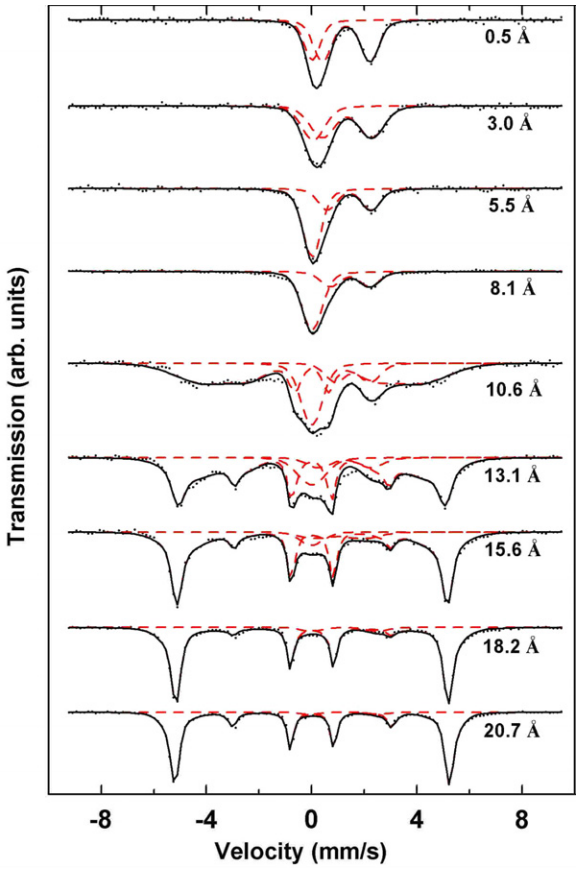

Figure 10. Room temperature ^{57}Fe Mössbauer spectra of the LiF/Fe multilayer library as a function of Fe content. The velocity scale is measured relative to room temperature α-Fe. The thickness of the Fe sublayer is shown below each spectrum. Solid lines through the data represent the total fits and the dashed lines are the spectral components.

XRD pattern showed that good crystalline LiF was obtained. Although this does not prove that the Li:F ratio is exactly 1:1, it does indicate that the sputtered material is close to ideal. Therefore, we assume that in the sputtered LiF/Fe multilayer library, the total Li:F ratio is equal to 1. The site parameters of the Fe atoms in the center of the sublayers suggest there is no Li in those regions. Therefore the extra Li atoms must end up in the LiF side of the interface. Recently, Maier *et al* proposed that extra Li atoms may be stored in the Li_2O side of the interfaces within Ru/Li_2O [3, 6] nanocomposites. Their *ab initio* calculations show that a Ti/Li_2O interface with extra Li atoms stored within Li_2O will have lower energy than the Ti/Li_2O interface with extra Li atoms at the interface.

The Mössbauer spectra collected for samples with Fe sublayer thickness between 15.6 and 10.6 Å were fitted with a symmetric sextet, a singlet and a doublet. When the Fe sublayer thickness falls below 10.6 Å, each Mössbauer spectrum was fit to one singlet and a doublet. The parameters of these components are also listed in table 2. The singlet has zero center shift and was assigned to superparamagnetic Fe. The doublet still corresponds to Fe atoms in the interfacial region.

Figure 11 shows the structure of the LiF/Fe multilayers based on our Mössbauer analysis. The width of the Fe layer has been drawn to scale. A thin interface region exists between the Fe layer and the LiF layer. Since some Fe atoms in this region have F atom neighbors the 'excess' lithium ions are stored at the LiF side of the interface, while the corresponding electrons are delocalized at the Fe side of the interface. This model is in agreement with the interfacial charge storage model proposed by Maier's group [3–6].

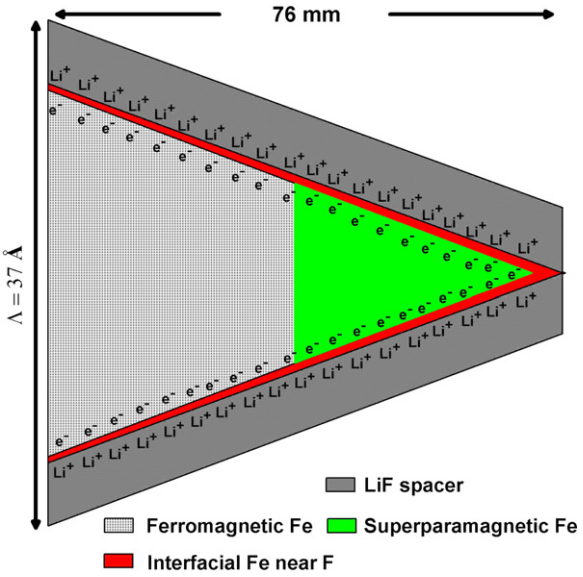

Figure 11. Schematic diagram of the structure of the LiF/Fe multilayer library. The width of the interfacial region and Fe layer were estimated from the site populations of the relative components in the Mössbauer spectra. The vertical and horizontal scales in the diagram are vastly different.

4. Conclusions

Ultrathin Al_2O_3/Fe and LiF/Fe multilayers were prepared by combinatorial magnetron sputtering. Their structural properties were analyzed by small angle x-ray scattering (SAXs), wide angle XRD and Mössbauer effect spectroscopy.

Interfacial regions were found in both systems based on the analysis of Mössbauer spectra. For the Al_2O_3/Fe multilayers, the sputtered Al_2O_3 was amorphous. A small number of Al atoms diffused into the Fe layer. Within the interfacial region, γ-Fe, $FeAl_2O_4$ as well as Fe atoms within amorphous Al_2O_3 were identified. For the LiF/Fe multilayers, a thin interfacial region exists between the Fe layers and the LiF layers. Mössbauer analysis shows that the Li:F ratio is less than 1 within the interfacial region, suggests that the 'excess' Li ions are located at the LiF side of the interface and also that the corresponding electrons are delocalized at the Fe side of the interface. This is consistent with Maier's interfacial charging hypothesis [3–6].

Acknowledgments

The authors acknowledge the support of this research by NSERC and 3M Canada under the auspices of the Industrial

Research Chair program. Special thanks are given to Dr Tim Hatchard for doing part of the Mössbauer experiments.

References

[1] Zhou Y N, Liu W Y, Xue M Z, Yu L, Wu C L, Wu X J and Fu Z W 2006 *Electrochem. Solid-State Lett.* **9** A147

[2] Liao P, Mar R and Dahn J R 2006 *210th Electrochemical Society Mtg (Cancun, Nov. 2006)* (Abstract 339)

[3] Maier J 2005 *Nat. Mater.* **4** 805

[4] Li H, Richter G and Maier J 2003 *Adv. Mater.* **15** 736

[5] Balaya P, Li H, Kienle L and Maier J 2003 *Adv. Funct. Mater.* **13** 621

[6] Zhukovskii Y F, Balaya P, Kotomin E A and Maier J 2006 *Phys. Rev. Lett.* **96** 058302

[7] Liao P, MacDonald B L, Dunlap R A and Dahn J R 2008 *Chem. Mater.* at press

[8] Mizushima K, Jones P C, Wiseman P J and Goodenough J B 1980 *Mater. Res. Bull.* **15** 783

[9] Li H, Balaya P and Maier J 2004 *J. Electrochem. Soc.* **151** A1878

[10] Makimura Y, Rougier A, Laffont L, Womes M, Jumas J-C, Leriche J-B and Tarascon J-M 2006 *Electrochem. Commun.* **8** 1769

[11] Poizot P, Laruelle S, Grugeon S, Dupont L and Tarascon J M 2000 *Nature* **407** 496

[12] Ochi M, Kita E, Saegusa N, Erata T and Tasaki A 1992 *J. Phys. Soc. Japan* **61** 35

[13] Kita E, Ochi M, Erata T and Tasaki A 1992 *J. Magn. Magn. Mater.* **117** 294

[14] Kaptás D, Balogh J, Kemény T, Kiss L F, Bujdosó L, Kovács A, Hirata A and Vincze I 2007 *Phys. Rev.* B **75** 014417

[15] Schmitt H, Stahl B, Ghafari M and Hahn H 2005 *J. Appl. Phys.* **97** 113902

[16] Lenoble O, Bauer Ph, Bobo J F, Fischer H, Ravet M F and Piecuch M 1994 *J. Phys.: Condens. Matter* **6** 3337

[17] Lenoble O, Bobo J F, Fischer H, Bauer Ph, Ravet M F and Piecuch M 1995 *J. Mater. Res.* **10** 3062

[18] Barkhouse D A R, Bonakdarpour A, Fleischauer M, Hatchard T D and Dahn J R 2003 *J. Magn. Magn. Mater.* **261** 399

[19] Dahn J R, Trussler S, Hatchard T D, Bonakdarpour A, Mueller-Neuhaus J R, Hewitt K C and Fleischauer M D 2002 *Chem. Mater.* **14** 3519

[20] Dunlap R A, Deschamps N C, Mar R E and Farrell S P 2006 *J. Phys.: Condens. Matter* **18** 4907

[21] Fullerton E E, Schuller I K, Vanderstraeten H and Bruynseraede Y 1992 *Phys. Rev.* B **45** 9292

[22] Fullerton E E, Pearson J, Sowers C H and Bader S D 1993 *Phys. Rev.* B **48** 17432

[23] Dunlap R A, Lawther D W, Hargraves P and Sinclair P 1988 *J. Phys. F: Met. Phys.* **18** 2479

[24] Matteazzi P and Le Caër G 1992 *J. Am. Ceram. Soc.* **75** 2749

[25] Eelman D A, Dahn J R, Mackay G R and Dunlap R A 1998 *J. Alloys Compounds* **266** 234

[26] Shenoy G K and Wagner F E 1978 *Mössbauer Isomer Shifts* (Amsterdam: North-Holland)